Abdominal Radiology

Published online: 28 September 2018

Abdom Radiol (2019) 44:1323–1330
https://doi.org/10.1007/s00261-018-1788-5

Evaluation of texture analysis for the differential diagnosis of focal nodular hyperplasia from hepatocellular adenoma on contrast-enhanced CT images

Roberto Cannella,[1,2] Amir A. Borhani,[1] Marta I. Minervini,[3] Allan Tsung,[4] and Alessandro Furlan[1]

[1]Abdominal Imaging Division, Department of Radiology, University of Pittsburgh, 200 Lothrop Street, Pittsburgh, PA 15213, USA
[2]Section of Radiology - Di.Bi.Med, University Hospital "Paolo Giaccone", Via del Vespro 127, 90127 Palermo, Italy
[3]Division of Transplantation and Liver Pathology, Department of Anatomic Pathology, University of Pittsburgh, Pittsburgh, PA, USA
[4]Division of Hepatobiliary and Pancreatic Surgery, Department of Surgery, University of Pittsburgh, Pittsburgh, PA, USA

Abstract

Purpose: To explore the value of CT texture analysis (CTTA) for differentiation of focal nodular hyperplasia (FNH) from hepatocellular adenoma (HCA) on contrast-enhanced CT (CECT).
Methods: This is a retrospective, IRB-approved study conducted in a single institution. A search of the medical records between 2008 and 2017 revealed 48 patients with 70 HCA and 50 patients with 62 FNH. All lesions were histologically proven and with available pre-operative CECT imaging. Hepatic arterial phase (HAP) and portal venous phase (PVP) were used for CTTA. Textural features were extracted using a commercially available research software (TexRAD). The differences between textural parameters of FNH and HCA were assessed using the Mann–Whitney *U* test and the AUROC were calculated. CTTA parameters showing significant difference in rank sum test were used for binary logistic regression analysis. A p value < 0.05 was considered statistically significant.
Results: On HAP images, mean, mpp, and skewness were significantly higher in FNH than in HCA on unfiltered images ($p \leq 0.007$); SD, entropy, and mpp on filtered analysis ($p \leq 0.006$). On PVP, mean, mpp, and skewness in FNH were significantly different from HCA ($p \leq 0.001$) on unfiltered images, while entropy and kurtosis were significantly higher in FNH on filtered images ($p \leq 0.018$). The multivariate logistic regression analysis indicated that the mean, mpp, and entropy of medium-level and coarse-level filtered images on HAP were independent predictors for the diagnosis of HCA and a model based on all these parameters showed the largest AUROC (0.824).
Conclusions: Multiple explored CTTA parameters are significantly different between FNH and HCA on CECT.

Key words: Hepatocellular adenoma—Focal nodular hyperplasia—Texture analysis—Liver—Computer tomography

Focal nodular hyperplasia (FNH) and hepatocellular adenoma (HCA) are the second and third most common benign solid liver lesions, respectively, both predominately occurring in young women [1]. Differentiating these two lesions from each other has a high clinical relevance due to the different risk of complications and different clinical managements. While complications are very rare in FNH [2], hemorrhage and malignant transformation can be seen in HCA [1].

Multiphasic contrast-enhanced CT (CECT) imaging is often the first modality for the non-invasive characterization of liver lesions. Differentiation of HCA from FNH may be difficult on CECT imaging when characteristic features such as intralesional scar or intralesional fat are lacking [3]. The enhancement pattern of FNH may overlap with that of inflammatory-type HCA [4] both presenting as hyperenhancing lesions on hepatic

Correspondence to: Alessandro Furlan; *email:* furlana@upmc.edu

arterial phase. Therefore, additional imaging with gadoxetic acid enhanced MR or a liver biopsy is often required to reach a definitive diagnosis.

Texture analysis is an emerging imaging-based post-processing method that allows for quantification of tissue heterogeneity [5, 6]. There has been a surge in research application of CT texture analysis (CTTA) in recent years. Texture analysis allows for mathematical extraction of several quantitative parameters that reflect the distribution and relationship of pixel gray-level value within a region of interest (ROI), providing additional information that cannot be detected by the human eyes [5]. Several oncologic and non-oncologic applications of CTTA have been investigated for liver diseases. Previous works have shown correlation between CTTA and tumor histology, molecular profile [7], prognosis [8–13], and treatment response [6] in different neoplasms. Recent studies have also reported the value of CTTA to differentiate benign from malignant liver lesions [14]. However, research on the role of CTTA in differentiating benign liver lesions has been limited [15].

The purpose of our study was to explore the value of CTTA for the differentiation of FNH from HCA on CECT imaging.

Materials and methods

The institutional review board approved this HIPPA-compliant retrospective study. The requirement to obtain informed consent was waived.

Population

The surgical and pathology records between January 2008 and December 2017 were searched to identify patients fulfilling the following criteria: (i) age ≥ 18 years; (ii) at least one pathologically proven HCA or FNH; (iii) CECT of the abdomen performed within 6 months before biopsy or resection of the lesion. The initial search resulted in 119 patients (113 females and 6 males, mean age 39.2 years) with 161 lesions (90 HCA, 71 FNH). Twenty-nine lesions were excluded due to (i) poor visualization of the lesion margins (n = 12) or severe imaging artifacts (n = 1); (ii) the presence of intralesional hemorrhage or necrosis (n = 14); (iii) small size, i.e., axial diameter of less than 5 mm (n = 2) (Fig. 1).

The final population included in the study (Table 1) was made of 98 patients: 48 patients (47 females, 1 male, mean age 40.1 ± 11.6 years) with 70 HCAs and 50 patients (48 females, 2 males, mean age 38.4 ± 9.8 years) with 62 FNHs. Pathologic confirmation was obtained via percutaneous needle biopsy (23 HCA; 14 FNH) or hepatic resection (47 HCA, 48 FNH). HCAs were classified according to genotype/phenotype and immunohistochemical characteristics into (1) HNF1α-mutated (n = 10, 14.3%), (2) inflammatory (n = 37, 52.8%), (3) β-catenin mutated (n = 3, 4.3%), and (4) unclassified (n = 20, 28.6%) subtypes. The mean ± SD interval time between CECT and the pathological proof was 57 ± 41 days (range 0–135 days).

CECT technique

Post-contrast images were obtained during hepatic arterial phase (HAP, 20–30 s after injection of contrast agent determined by "bolus tracking" technique, using a threshold of 100 HU in the abdominal aorta) and portal venous phase (PVP, 30–40 s after the completion of HAP). The patients received 100–125 mL of Iopamidol (Isovue 370; Bracco Diagnostics, Princeton, NJ) or Iohexol (Omnipaque 350; GE Healthcare, Princeton, NJ) injected through a peripheral intravenous line at rate of 3–5 mL/s. The scanning parameters were as follows: slice thickness, 3–5 mm; pitch, 1.375; tube potential, 120 kVp; automatic mA modulation with range of 100–590 mA; matrix size, 512 × 512; and field of view, 327–500 mm. Unenhanced CT images were acquired only in 30% of the studies and thus not included in the TA.

Texture analysis

Texture analysis was performed by a single observer (R.C.) with 4 years of experience in cross-sectional imaging and 6 months of experience with texture analysis, blinded to the pathological classification. The study coordinator (A.F.) reviewed the surgical reports and the ultrasound images obtained during percutaneous biopsy to ensure only pathologically proven lesions were included in the study.

The CT images were anonymized and exported to a dedicated workstation for CTTA. Textural features were extracted using a commercially available research software (TexRAD, version 3.9, Feedback Plc, Cambridge, UK) which applies a two-step filtration-histogram approach. Axial HAP and PVP images were used for texture analysis. A polygonal ROI was manually drawn on the largest cross section within the margins of the lesions as described in prior studies (Figs. 2, 3) [8, 9, 16]. A 2-cm rounded ROI was also placed on the non-lesional right lobe liver parenchyma. In each post-contrast phase, the software automatically extracts an independent dataset of texture parameters based on the histogram of gray-level frequency and gray-level distribution within the region of interest. Statistical and histogram-based parameters were extracted before and following the application of different levels of filtration by using Laplacian of Gaussian spatial band-pass filter. Each filter (spatial scale filter, SSF) highlights the features of objects with a specific size (object radii of 2–6 mm). The

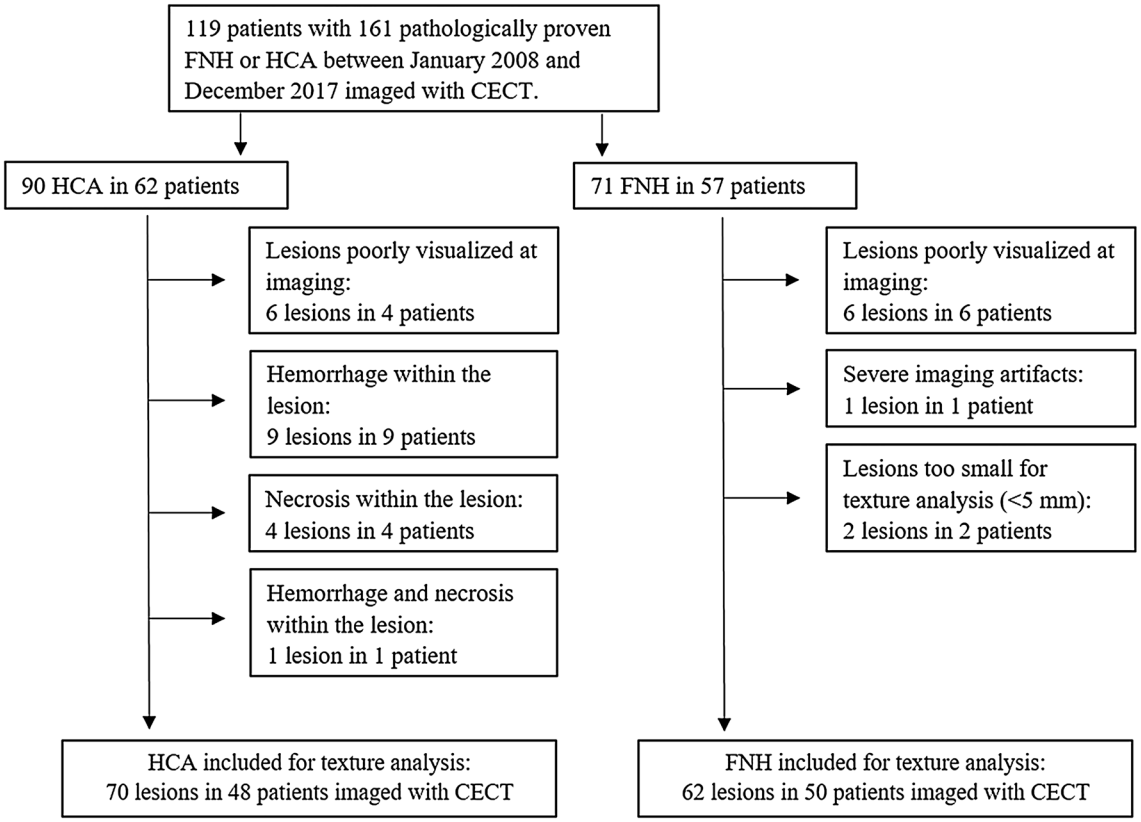

Fig. 1. Flow diagram for the selection of the final population with hepatocellular adenoma (HCA) or focal nodular hyperplasia (FNH).

Table 1. Characteristic of the final population

Baseline characteristics	FNH (50 patients with 62 lesions)	HCA (48 patients with 70 lesions)
Patients' gender		
Females	48 (96.0)	47 (97.9)
Males	2 (4.0)	1 (2.1)
Patients' age	Mean 38.4 ± 9.8 years (range 18–58)	Mean 40.1 ± 11.65 years (range 18–61)
Pathologic confirmation		
Biopsy	14 (22.6)	23 (32.9)
Resection	48 (77.4)	47 (67.1)
Lesions size	4.7 ± 3.0 cm (range 0.8 - 12.2 cm)	4.2 ± 2.8 cm (range 1.0 - 11.2 cm)
Patients' number of lesions		
Single	31	19
Multiple	19 (mean 3; range 2–6)	29 (mean 13, range 2–27)

unfiltered parameters are labeled as SSF = 0. Filter value of 2 mm (SSF = 2) indicates fine texture; filters of 3 and 4 mm (SSF = 3 or 4) correspond to medium texture, and filters of 5 and 6 mm (SSF = 5 or 6) indicate coarse texture. Histogram parameters included for this study were mean (average value of the pixels), standard deviations (SD), entropy (indicator of irregularity) [5, 17], mean of positive pixel (mpp), skewness (indicating asymmetry of the histogram), and kurtosis (indicating peakedness of the histogram) [18].

Statistical analysis

The Mann–Whitney *U* test was used to compare the distribution of CTTA parameters in HCAs and FNHs. Receiver operating characteristics (ROC) analyses were performed for the most discriminative features to assess the performance for the diagnosis of HCA. CTTA parameters which were shown to be statistically significant were then entered in a binary logistic regression (forward conditional). In addition, an exploratory anal-

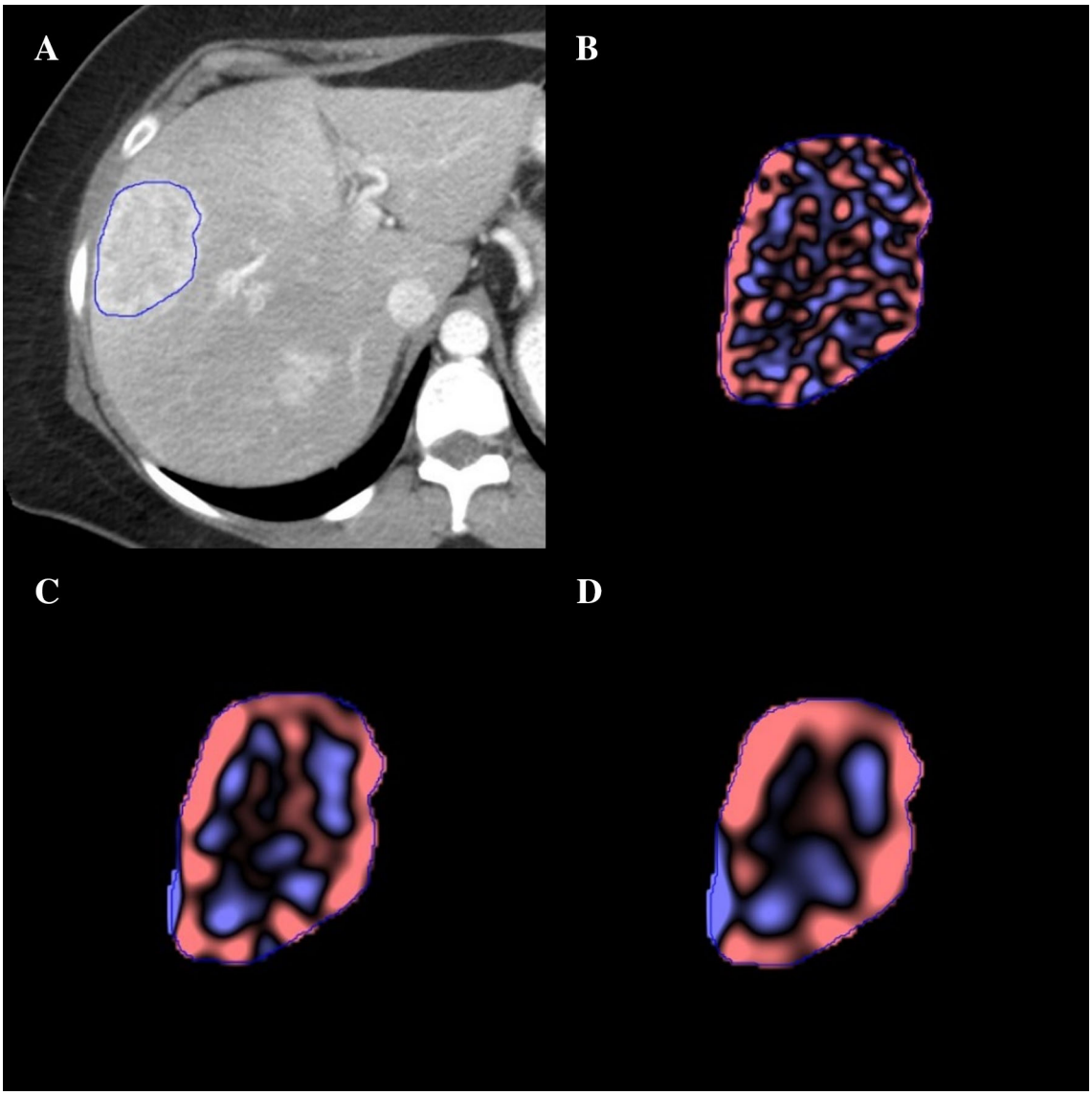

Fig. 2. Texture analysis on a 30-year-old female with inflammatory hepatocellular adenoma. A polygonal ROI was manually drawn within the margin of the lesion (**A**) on HAP. Representative images of texture features extracted with fine (SFF = 2, **B**), medium (SSF = 4, **C**), and coarse (SSF = 6, **D**) filters.

ysis of the role of CT texture analysis for the differentiation of the subtypes of HCA was conducted using Kruskall–Wallis test.

Statistical significance level was set at $p < 0.05$. Statistical analysis was conducted using SPSS software (version 18.0; SPSS, Chicago, IL) and MedCalc for Windows, version 17.1 (MedCalc Software, Ostend, Belgium).

Results

On HAP images, multiple CTTA parameters were statistically higher in FNH compared to HCA (Table 2). The strongest differences on unfiltered images were found for mean, mpp, and skewness ($p \leq 0.007$); on medium-level filter for SD ($p \leq 0.006$); and on coarse-level filter for SD, entropy, and mpp ($p \leq 0.003$). The largest calculated AUROCs for the diagnosis of HCA were for mean on 5-mm coarse filter (0.638; CI 0.535–0.733), mpp on 6-mm coarse filter (0.681; CI 0.579–0.771), entropy on 4-mm medium-level filter (0.646; CI 0.543–0.740), and 6-mm coarse-level filter (0.707; CI 0.606–0.794). These four parameters were independent predictors of HCA at logistic regression analysis. A combined model based on all these CTTA features yielded a AUROC of 0.824 (CI 0.734–0.894) (Fig. 4).

On PVP images, mean, mpp, and skewness were statistically different on unfiltered images ($p \leq 0.001$) (Table 3). The corresponding AUROC for the diagnosis of HCA were 0.678 (CI 0.590–0.757) for the mean, 0.679

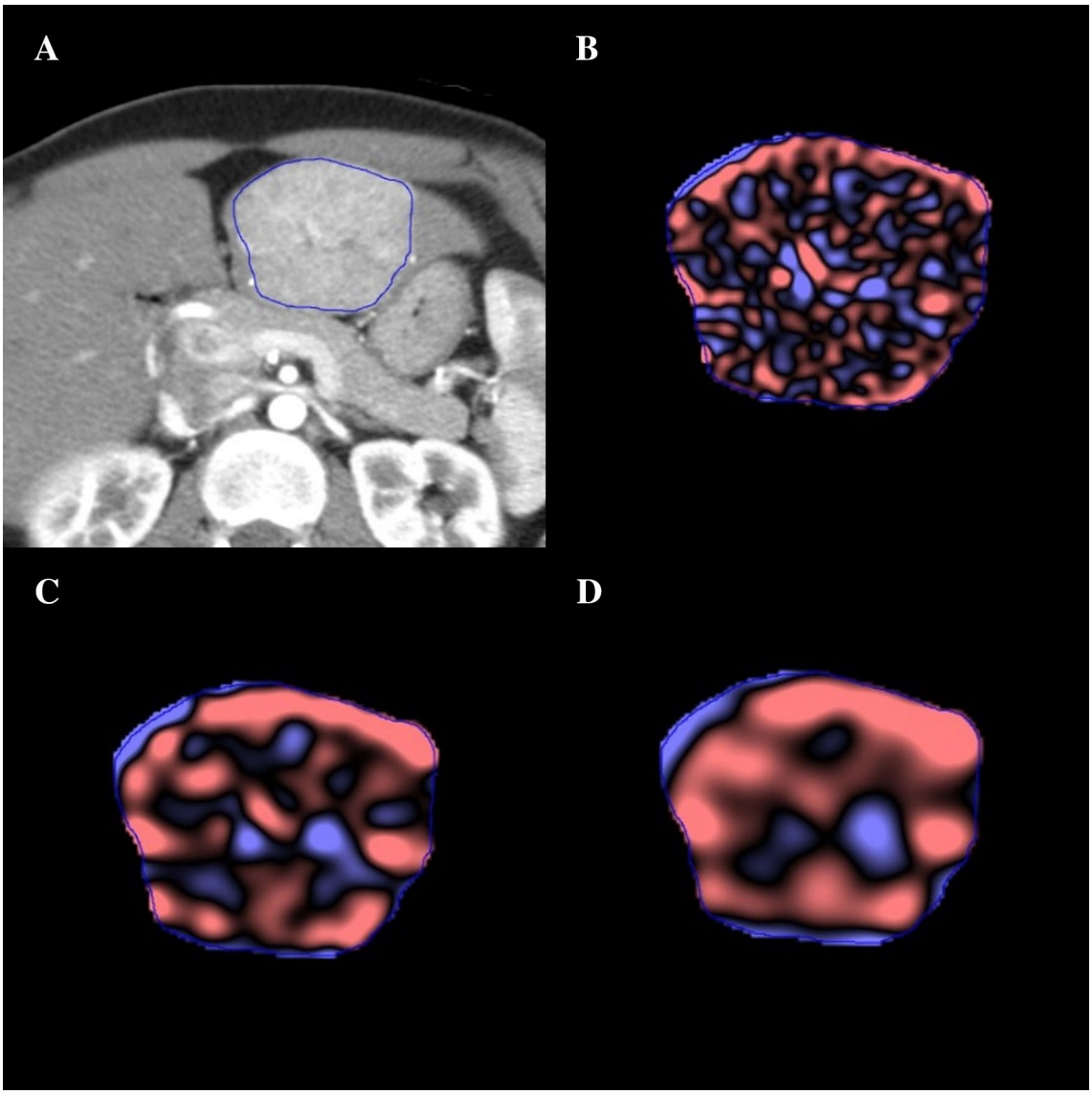

Fig. 3. Texture analysis on a 41-year-old-female patient with focal nodular hyperplasia. Representative images of the ROI drawn on HAP (**A**) and texture features extracted with fine (SFF = 2, **B**), medium (SSF = 4, **C**), and coarse (SSF = 6, **D**) filters.

(CI 0.591–0.758) for mpp, and 0.674 (CI 0.586–0.753) for skewness. When applying fine- and medium-level filters, the kurtosis was statistically higher in FNH ($p \leq 0.001$), while entropy was significantly higher in both 5-mm and 6-mm coarse filters ($p = 0.018$). On filtered images, the largest AUROC curve was for the kurtosis on 2-mm fine filter (0.678; CI 0.590–0.757). The logistic regression analysis demonstrated that mean and skewness were independent predictor for the diagnosis of HCA. A model based on these two parameters yielded a AUROC of 0.733 (CI 0.648–0.807) (Fig. 5).

We also explored the potential of texture analysis in differentiating the four subgroups of HCA, but none of the texture parameters was statistically different. The analysis of non-lesional liver did not show any significantly difference on the texture parameters extracted from the right hepatic lobe.

Discussion

We explored the diagnostic performance of texture analysis on CECT in differentiating HCA from FNH. Multiple CTTA parameters showed a significantly different distribution between HCAs and FNHs on both filtered and unfiltered images. While the AUROC of each single parameter was relatively low, models based on the combination of parameters showed a fair-to-good diagnostic accuracy on HAP (AUROC, 0.824) and PVP (AUROC, 0.733) images.

Differentiating HCA from FNH has clear clinical importance. While FNH requires a conservative man-

Table 2. CTTA parameters on HAP with a statistically significant different distribution between FNHs and HCAs in filtered and unfiltered images

Texture parameters	FNH	HCA	*p*
SSF = 0 (unfiltered)			
Mean	115.72 ± 32.50	96.57 ± 34.41	0.002
mpp	115.78 ± 32.44	96.62 ± 34.36	0.002
Skewness	− 0.23 ± 0.45	− 0.08 ± 0.29	0.007
Kurtosis	0.73 ± 1.85	0.16 ± 0.70	0.047
SSF = 2 (fine filter)			
Mean	26.21 ± 25.90	14.83 ± 17.02	0.007
SSF = 3 (medium filter)			
Mean	42.56 ± 40.21	24.94 ± 27.66	0.015
SD	55.16 ± 18.56	45.80 ± 19.00	0.006
mpp	64.10 ± 36.07	49.40 ± 24.49	0.017
SSF = 4 (medium filter)			
Mean	56.84 ± 50.05	33.68 ± 36.85	0.020
SD	57.94 ± 22.56	45.11 ± 20.86	0.001
Entropy	5.08 ± 0.37	4.85 ± 0.47	0.013
mpp	76.11 ± 45.07	55.10 ± 30.15	0.008
SSF = 5 (coarse filter)			
Mean	68.51 ± 55.47	40.61 ± 44.57	0.018
SD	60.35 ± 23.77	44.65 ± 22.11	< 0.001
Entropy	5.10 ± 0.39	4.82 ± 0.48	0.002
mpp	86.56 ± 49.67	59.91 ± 33.70	0.003
Skewness	− 0.38 ± 0.61	− 0.20 ± 0.86	0.016
SSF = 6 (coarse filter)			
Mean	77.40 ± 57.70	46.16 ± 51.55	0.014
SD	62.09 ± 24.02	44.39 ± 23.37	< 0.001
Entropy	5.14 ± 0.39	4.80 ± 0.49	< 0.001
mpp	94.78 ± 51.16	65.23 ± 38.06	0.002
Skewness	− 0.46 ± 0.52	− 0.27 ± 0.77	0.016

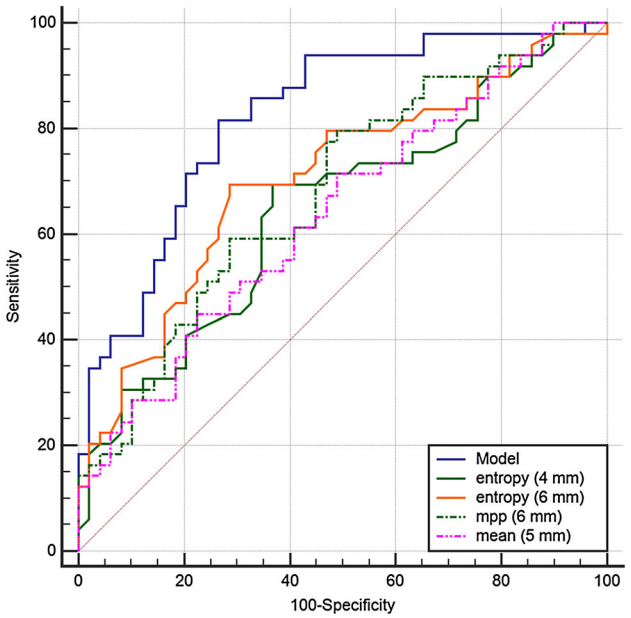

Fig. 4. Receiver operating curves of mean (5 mm coarse), mpp (6-mm coarse filter), entropy (4-mm medium and 6-mm coarse filters), and logistic regression analysis model for the diagnosis of hepatocellular adenoma on hepatic arterial phase.

agement [19], HCA may need a more careful imaging follow-up or surgical resection given the risk of hemorrhage (symptomatic bleeding in 14% of cases) [1] and

Table 3. CTTA parameters on PVP with a statistically significant different distribution between FNHs and HCAs in filtered and unfiltered images

Texture parameters	FNH	HCA	*p*
SSF = 0 (unfiltrered)			
Mean	121.80 ± 25.14	103.87 ± 29.52	< 0.001
mpp	121.90 ± 25.00	103.88 ± 29.51	< 0.001
Skewness	− 0.27 ± 0.46	0.0034 ± 0.22	0.001
Kurtosis	0.83 ± 1.58	0.079 ± 0.36	0.004
SSF = 2 (fine filter)			
Mean	9.90 ± 17.89	2.35 ± 16.57	0.041
Kurtosis	1.34 ± 1.95	0.52 ± 2.01	< 0.001
SSF = 3 (medium filter)			
Mean	17.18 ± 29.29	4.33 ± 26.71	0.041
SD	42.33 ± 15.08	37.74 ± 13.40	0.030
Kurtosis	2.10 ± 2.78	1.10 ± 3.22	0.001
SSF = 4 (medium filter)			
Mean	23.99 ± 38.50	6.77 ± 35.39	0.031
SD	44.58 ± 18.96	38.57 ± 16.27	0.018
Entropy	4.82 ± 0.36	4.70 ± 0.36	0.024
SSF = 5 (coarse filter)			
Mean	29.97 ± 44.75	9.86 ± 42.23	0.032
SD	46.99 ± 22.14	39.63 ± 19.11	0.020
Entropy	4.83 ± 0.41	4.69 ± 0.40	0.018
mpp	51.09 ± 41.93	38.88 ± 23.72	0.045
SSF = 6 (coarse filter)			
Mean	34.86 ± 48.18	13.53 ± 47.31	0.049
SD	48.40 ± 24.81	39.65 ± 20.95	0.023
Entropy	4.84 ± 0.47	4.68 ± 0.45	0.018
mpp	55.34 ± 44.94	41.34 ± 27.52	0.032
Skewness	− 0.16 ± 0.94	0.13 ± 0.75	0.041

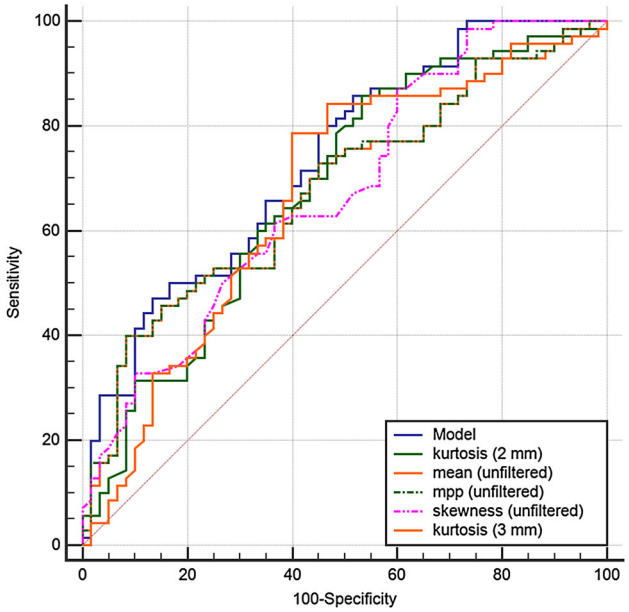

Fig. 5. Receiver operating curves of unfiltered mean, mpp and skewness, fine (2 mm) and medium (3 mm) filtered kurtosis, and logistic regression analysis model for the diagnosis of hepatocellular adenoma on portal venous phase.

malignant transformation (4.2%) [20]. CECT is often the first imaging modality for the characterization of liver lesions. However, distinguishing an FNH from a HCA on CECT remains challenging especially when they lack typical imaging features such as a central scar, suggestive of FNH (reported in about 50% of FNHs larger than 3 cm [21]) or intralesional fat, suggestive of HCA. CECT imaging has a reported diagnostic accuracy ranging from 50 to 70% for diagnosis of FNH with typical imaging presentation [22–25]. The appearance of FNH and HCA on CECT may overlap. The classic appearance of FNH is an intense and homogeneous enhancement on HAP fading on PVP [26, 27]. HCA may also present as a hypervascular lesion with various degree of enhancement and with fading or washout on PVP, depending of the subtype [28, 29]. Particularly, inflammatory HCAs are characterized by marked arterial phase hyperenhancement fading on PVP and delayed phases, thus overlapping with the appearance of an FNH [4]. As a result, a liver MRI with hepatobiliary contrast agent (Gd-BOPTA, Gd-EOB-DTPA) is usually required for definitive characterization given the high diagnostic accuracy (sensitivity of 92% and specificity of 95% for the lesions demonstrating hypointensity on hepatobiliary phase) [30, 31].

By quantification of lesion heterogeneity, CTTA can potentially help with differentiation of these two types of lesions. The difference in texture parameters reported in our study between FNHs and HCAs may reflect the different histopathology of these lesions. The higher heterogeneity of FNH (better manifested by higher mean, mpp and entropy on HAP) may be related to the presence of thick irregular fibrous septae dividing the mass into multiple nodules/segments and large dystrophic arteries [32], a spatial organization not seen on HCA. To the best of our knowledge, only one other study [15] has investigated the value of CT texture analysis in differentiating hypervascular liver lesions, including FNH and HCA, in which a total of 17 FNH and 19 HCA were evaluated among a larger cohort of 61 hypervascular lesions. In that study, the only statistically different texture parameter between FNH and HCA was the mean in medium (3 mm and 4 mm) and coarse filters (5 mm and 6 mm). Only HAP images were analyzed in the aforementioned study and the immunohistochemical classification of the HCAs was not reported. Moreover, not all FNHs were pathologically proven. The current study is concordant with the prior investigation showing that the mean on HAP images with coarse filter was statistically higher in FNH than in HCA with an AUROC of 0.638.

HCA is a diverse entity that can be divided into four main subgroups according to the histopathological and immunohistochemical classification [33]: (1) HNF1α-mutated HCA (occurring in 35–40% of cases); (2) inflammatory HCA (40–50%); (3) β-catenin mutated HCA (10%); and (4) unclassified HCA (10%). None of the texture parameters was statistically different among the subtypes of HCA on HAP and PVP images. This could be explained by relatively smaller number of HNF1α-mutated (n = 10, 14.3%) and β-catenin-mutated (n = 3, 4.3%) HCAs compared to inflammatory HCA (n = 37, 52.8%) in our cohort. Moreover, CT images have a lower contrast resolution compared to other imaging technique (i.e., Magnetic Resonance) and this could limit the quantification of heterogeneity in HCA subtypes.

We acknowledge the following limitations in our study. Firstly, it was conducted retrospectively over a long period of time (10 years) that may have affected homogeneity of CT acquisitions technique. However, previous studies have demonstrated that CTTA parameters are not significantly influenced by the variations of acquisition parameters and different CT scanners [10, 34] with a good inter-reader agreement [9]. Secondly, only pathological proven lesions were included in our cohort. Although this step is a necessary inclusion criterion to validate the correlation between texture parameters and different histological classification, it may constitute a selection bias due to the lower number of FNH than HCA.

In conclusion, multiple explored CTTA parameters are significantly different in FNH compared to HCA. These results justify further larger-cohort studies, preferably multicenter, to validate the use of texture analysis in differentiating benign liver lesions and to increase the diagnostic value of CECT.

Compliance with ethical standards

Funding No funding was received for this study.

Conflict of interest The authors declare that they have no conflict of interests.

Disclosure Alessandro Furlan: research grant from General Electric; consultant for General Electric; book contract with Elsevier/Amirsys. Amir A. Borhani: consultant for Guebert; consultant for Elsevier/Amirsys.

Ethical approval All procedures performed in studies involving human participants were in accordance with the ethical standards of the institutional and/or national research committee and with the 1964 Helsinki declaration and its later amendments or comparable ethical standards.

Informed consent For this type of study formal consent is not required.

References

1. Nault JC, Couchy G, Balabaud C, et al. (2017) Molecular classification of hepatocellular adenoma associates with risk factors, bleeding, and malignant transformation. Gastroenterology 152(880–894):e6
2. Navarro AP, Gomez D, Lamb CM, Brooks A, Cameron IC (2014) Focal nodular hyperplasia: a review of current indications for and outcomes of hepatic resection. HPB (Oxford) 16:503–511
3. Ruppert-Kohlmayr AJ, Uggowitzer MM, Kugler C, et al. (2001) Focal nodular hyperplasia and hepatocellular adenoma of the liver: differentiation with multiphasic helical CT. AJR Am J Roentgenol 176:1493–1498
4. Agarwal S, Fuentes-Orrego JM, Arnason T, et al. (2014) Inflammatory hepatocellular adenomas can mimic focal nodular hyperplasia on gadoxetic acid-enhanced MRI. AJR Am J Roentgenol 203:W408–W414
5. Davnall F, Yip CS, Ljungqvist G, et al. (2012) Assessment of tumor heterogeneity: an emerging imaging tool for clinical practice? Insights Imaging 3:573–589
6. Ganeshan B, Miles KA (2013) Quantifying tumour heterogeneity with CT. Cancer Imaging 13:140–149
7. Sadot E, Simpson AL, Do RK, et al. (2015) Cholangiocarcinoma: correlation between molecular profiling and imaging phenotypes. PLoS ONE 10:e0132953
8. Kiryu S, Akai H, Nojima M, et al. (2017) Impact of hepatocellular carcinoma heterogeneity on computed tomography as a prognostic indicator. Sci Rep 7:12689
9. Mulé S, Thiefin G, Costentin C, et al. (2018) Advanced hepatocellular carcinoma: pretreatment contrast-enhanced CT texture parameters as predictive biomarkers of survival in patients treated with sorafenib. Radiology 288:445–455
10. Miles KA, Ganeshan B, Griffiths MR, Young RC, Chatwin CR (2009) Colorectal cancer: texture analysis of portal phase hepatic CT images as a potential marker of survival. Radiology 250:444–452
11. Ahn SJ, Kim JH, Park SJ, Han JK (2016) Prediction of the therapeutic response after FOLFOX and FOLFIRI treatment for patients with liver metastasis from colorectal cancer using computerized CT texture analysis. Eur J Radiol 85:1867–1874
12. Beckers RCJ, Lambregts DMJ, Schnerr RS, et al. (2017) Whole liver CT texture analysis to predict the development of colorectal liver metastases—a multicentre study. Eur J Radiol 92:64–71
13. Lubner MG, Stabo N, Lubner SJ, et al. (2015) CT textural analysis of hepatic metastatic colorectal cancer: pre-treatment tumor heterogeneity correlates with pathology and clinical outcomes. Abdom Imaging 40:2331–2337
14. Chang CC, Chen HH, Chang YC, et al. (2017) Computer-aided diagnosis of liver tumors on computed tomography images. Comput Methods Progr Biomed 145:45–51
15. Raman SP, Schroeder JL, Huang P, et al. (2015) Preliminary data using computed tomography texture analysis for the classification of hypervascular liver lesions: generation of a predictive model on the basis of quantitative spatial frequency measurements–a work in progress. J Comput Assist Tomogr 39:383–395
16. Chen S, Zhu Y, Liu Z, Liang C (2017) Texture analysis of baseline multiphasic hepatic computed tomography images for the prognosis of single hepatocellular carcinoma after hepatectomy: a retrospective pilot study. Eur J Radiol 90:198–204
17. Ganeshan B, Miles KA, Young RC, Chatwin CR (2007) Hepatic entropy and uniformity: additional parameters that can potentially increase the effectiveness of contrast enhancement during abdominal CT. Clin Radiol 62:761–768
18. Miles KA, Ganeshan B, Hayball MP (2013) CT texture analysis using the filtration-histogram method: what do the measurements mean? Cancer Imaging 13:400–406
19. Perrakis A, Demir R, Müller V, et al. (2012) Management of the focal nodular hyperplasia of the liver: evaluation of the surgical treatment comparing with observation only. Am J Surg 204:689–696
20. Stoot JH, Coelen RJ, De Jong MC, Dejong CH (2010) Malignant transformation of hepatocellular adenomas into hepatocellular carcinomas: a systematic review including more than 1600 adenoma cases. HPB (Oxford) 12:509–522
21. Brancatelli G, Federle MP, Grazioli L, et al. (2001) Focal nodular hyperplasia: CT findings with emphasis on multiphasic helical CT in 78 patients. Radiology 219:61–68
22. Nowicki TK, Markiet K, Izycka-Swieszewska E, et al. (2018) Efficacy comparison of multi-phase CT and hepatotropic contrast-enhanced MRI in the differential diagnosis of focal nodular hyperplasia: a prospective cohort study. BMC Gastroenterol. 18:10
23. Shen YH, Fan J, Wu ZQ, et al. (2007) Focal nodular hyperplasia of the liver in 86 patients. Hepatobiliary Pancreat Dis Int 6:52–57
24. Bonney GK, Gomez D, Al-Mukhtar A, et al. (2007) Indication for treatment and long-term outcome of focal nodular hyperplasia. HPB (Oxford) 9:368–372
25. Choi CS, Freeny PC (1998) Triphasic helical CT of hepatic focal nodular hyperplasia: incidence of atypical findings. AJR Am J Roentgenol 170:391–395
26. Carlson SK, Johnson CD, Bender CE, Welch TJ (2000) CT of focal nodular hyperplasia of the liver. AJR Am J Roentgenol 174:705–712
27. Winterer JT, Kotter E, Ghanem N, Langer M (2006) Detection and characterization of benign focal liver lesions with multislice CT. Eur Radiol 16:2427–2443
28. Hussain SM, van den Bos IC, Dwarkasing RS, Kuiper JW, den Hollander J (2006) Hepatocellular adenoma: findings at state-of-the-art magnetic resonance imaging, ultrasound, computed tomography and pathologic analysis. Eur Radiol 16:1873–1886
29. Ichikawa T, Federle MP, Grazioli L, Nalesnik M (2000) Hepatocellular adenoma: multiphasic CT and histopathologic findings in 25 patients. Radiology 214:861–868
30. McInnes MD, Hibbert RM, Inácio JR, Schieda N (2015) Focal nodular hyperplasia and hepatocellular adenoma: accuracy of gadoxetic acid-enhanced MR imaging—a systematic review. Radiology 277:413–423
31. Guo Y, Li W, Xie Z, et al. (2017) Diagnostic value of Gd-EOB-DTPA-MRI for Hepatocellular adenoma: a meta-analysis. J Cancer 8:1301–1310
32. Balabaud C, Al-Rabih WR, Chen PJ, et al. (2013) Focal nodular hyperplasia and hepatocellular adenoma around the world viewed through the scope of the immunopathological classification. Int J Hepatol 2013:268625
33. Bioulac-Sage P, Rebouissou S, Thomas C, et al. (2007) Hepatocellular adenoma subtype classification using molecular markers and immunohistochemistry. Hepatology 46:740–748
34. Yasaka K, Akai H, Mackin D, et al. (2017) Precision of quantitative computed tomography texture analysis using image filtering: a phantom study for scanner variability. Medicine (Baltimore) 96:e6993